

Strong Coupling between Magnons and Microwave Photons in On-Chip Ferromagnet-Superconductor Thin-Film Devices

Yi Li,^{1,2} Tomas Polakovic,^{3,4} Yong-Lei Wang,^{2,5} Jing Xu,^{2,6} Sergi Lendinez,² Zhizhi Zhang,^{2,7} Junjia Ding,² Trupti Khaire,² Hilal Saglam,^{2,8} Ralu Divan,⁹ John Pearson,² Wai-Kwong Kwok,² Zhili Xiao,^{2,6} Valentine Novosad,^{2,*} Axel Hoffmann,^{2,†} and Wei Zhang^{1,2,‡}

¹*Department of Physics, Oakland University, Rochester, Michigan 48309, USA*

²*Materials Science Division, Argonne National Laboratory, Argonne, Illinois 60439, USA*

³*Physics Division, Argonne National Laboratory, Argonne, Illinois 60439, USA*

⁴*Department of Physics, Drexel University, Philadelphia, Pennsylvania 19104, USA*

⁵*Research Institute of Superconductor Electronics, School of Electronic Science and Engineering, Nanjing University, 210093, Nanjing, China*

⁶*Department of Physics, Northern Illinois University, DeKalb, Illinois 60115, USA*

⁷*School of Optical and Electronic Information, Huazhong University of Science and Technology, Wuhan 430074, China*

⁸*Department of Physics, Illinois Institute of Technology, Chicago Illinois 60616, USA*

⁹*Center for Nanoscale Materials, Argonne National Laboratory, Argonne, Illinois 60439, USA*

 (Received 25 February 2019; published 3 September 2019)

We demonstrate strong magnon-photon coupling of a thin-film Permalloy device fabricated on a coplanar superconducting resonator. A coupling strength of 0.152 GHz and a cooperativity of 68 are found for a 30-nm-thick Permalloy stripe. The coupling strength is tunable by rotating the biasing magnetic field or changing the volume of Permalloy. We also observe an enhancement of magnon-photon coupling in the nonlinear regime of the superconducting resonator, which is attributed to the nucleation of dynamic flux vortices. Our results demonstrate a critical step towards future integrated hybrid systems for quantum magnonics and on-chip coherent information transfer.

DOI: [10.1103/PhysRevLett.123.107701](https://doi.org/10.1103/PhysRevLett.123.107701)

Hybrid systems play a crucial role in quantum information processing [1–3]. In these systems, quantum states are coherently conveyed from one platform to another, with diverse carriers such as superconducting qubits, optical and microwave photons, individual atoms, ions, spin ensembles, and phonons [4–10]. This coherent transduction, which is represented by its mode hybridization [11], will be necessary to utilize the advantage of different state variables while maintaining the quantum coherence and entanglements.

Recently, magnons have been considered as a new candidate for coherent information processing [12–26]. Magnons are the collective excitation of exchange-coupled spins in magnetic materials. They can conveniently couple to microwave photons via dipolar interaction. Especially, compared with paramagnetic spin ensembles which have been proposed as quantum memories [6,7,27–29], magnetic materials can provide much larger coupling strength and cooperativity, because they have spin densities 4 to 6 orders of magnitude higher than in spin ensembles [13]. This means magnons are capable of exchanging information with a much faster speed and for more cycles before losing coherency, while keeping the device dimension small. Coherent coupling between superconducting qubits and a single magnon has also been recently demonstrated

[18,24], showing the potential for magnons to conduct real quantum operations. Furthermore, with new advances in spin-charge interconversion [30,31], the excitation of magnons in hybrid systems can be electrically detected via spin pumping [19,21,32] and potentially other spin-transport phenomena [33,34].

Despite the progress in magnon-photon hybrid systems, which are predominantly centered on yttrium iron garnet (YIG) ferrimagnets [13–20,22–26], the crucial step for extended development, i.e., on-chip integration and miniaturization, are problematic for YIG because of the critical conditions in deposition and fabrication. The standard substrate for growing YIG, $\text{Gd}_3\text{Ga}_5\text{O}_{12}$, experience large magnetic losses at cryogenic temperatures [35] and will reduce the coherency for quantum applications. In addition, maximizing coupling efficiency between magnons and microwave photons requires good proximity between magnetic spins and microwave resonator, which will be ideal if the magnetic devices are confined and directly fabricated on the resonator. Thus it is desirable to explore alternative magnetic systems for large-scale magnon-based hybrid quantum systems.

In this work, we demonstrate an all-on-chip magnon-photon hybrid circuit with a Permalloy ($\text{Ni}_{80}\text{Fe}_{20}$, Py) thin-film device directly fabricated on top of a coplanar

superconducting resonator. On the magnon side, Py is a classical metallic ferromagnet with well-known magnetic properties and industry-friendly deposition requirements. It exhibits 5 times larger spin density than YIG and allows even larger coupling strengths. On the photon side, a coplanar superconducting resonator has a much smaller mode volume and a higher quality factor than a macroscopic microwave cavity, which allows more concentrated and long-lived photons to couple with magnons. We achieve a strong magnon-photon coupling strength of $g/2\pi = 0.152$ GHz and cooperativity of $C = 68$ for a 30-nm-thick Py stripe (total volume $V = 400 \mu\text{m}^3$), along with a high coupling efficiency of 26.7 Hz per Bohr magneton. Furthermore, the coupling strength can be further enhanced by driving the superconducting resonator into the nonlinear regime, which is attributed to the creation of dynamic magnetic flux vortices. Our results suggest the combination of superconducting resonator and metallic ferromagnets can be a promising platform for investigating on-chip quantum magnonics and spintronics, and brings new potential for coherent manipulation and long-distance propagation of spin information.

Superconducting coplanar resonators were fabricated [36] from 200-nm-thick NbN films by photolithography and reactive ion etching, Fig. 1(a). The NbN films were deposited on undoped Si substrates via reactive sputtering techniques at room temperature [37]. Subsequently, a 30-nm Py thin-film stripe with lateral dimensions of $14 \times 900 \mu\text{m}^2$ was fabricated on top of the signal line of the

resonator but electrically isolated from it by a 20-nm MgO insulating layer. The microwave response of the system was characterized by a vector network analyzer. Throughout the experiment the samples were cooled down to 1.4 K, which is well below the superconducting transition temperature of the NbN resonator, $T_c = 14$ K [38].

The mode evolution of the individual magnon and photon systems are shown in Figs. 1(c) and 1(d), respectively, as a function of the in-plane magnetic field H_B along the stripline orientation [$\theta = 0^\circ$, defined in Fig. 1(a)]. For the photon subsystem (without the Py stripe), the NbN resonator exhibits a sharp peak at $\omega_p/2\pi = 5.069$ GHz with a full width half maximum linewidth $\Delta\omega_p/2\pi = 0.67$ MHz, corresponding to a high quality factor of $Q = 7600$, see Fig. 1(b). The peak position corresponds to a dielectric constant, $\epsilon_r \sim 9.3$, similar to the value of 11.7 for Si. In addition, we obtain a hysteresis of ω_p by sweeping H_B [Fig. 1(c)]. This behavior originates from the kinetic inductance variation from magnetic flux vortices in superconducting resonators [39]. For the magnon subsystem, we have fabricated an individual Py stripe on a coplanar waveguide and measured its broadband ferromagnetic resonance at 1.4 K [38]. Two branches of resonance absorption are symmetrically located on the positive and negative fields, as shown in Fig. 1(d). The small field offset, ~ 5 mT, comes from the hysteresis of the superconducting magnet coils. From Fig. 1(d), we can determine the magnon damping rate as $\kappa_m/2\pi = 0.178$ GHz.

We then turn to the magnon-photon hybridization. Before the Py deposition, the superconducting resonator exhibits a continuous spectra when $\mu_0 H_B$ is swept from -100 to 100 mT, as shown in Fig. 2(a). After Py deposition, two avoided crossings appear symmetrically at positive and negative $\mu_0 H_B$ [Fig. 2(b)]. The mode anticrossing indicates a strong coupling between the resonator photons and the ferromagnetic magnons. We also observe a broad resonance at 5.00 GHz for Fig. 2(a) and 4.88 GHz for Fig. 2(b), both independent of H_B . They come from spurious resonances of the microwave circuits and are not relevant to the mode hybridization. The extracted peak positions (ω_{mp}) and linewidths ($\Delta\omega_{mp}$) of the spectra are summarized in Figs. 2(c) and 2(d), respectively. A frequency offset of 0.12 GHz between Figs. 2(a) and 2(b) have been taken into account due to the local impedance change from the additional Py stripe. As shown in Fig. 2(c), the two anticrossings are located where the two magnon branches of the Py stripe intersect with the photon mode of the resonator, which clearly indicates the strong magnon-photon coupling.

The transmitted power of the hybrid system can be expressed as [13–15,19]

$$\frac{P_{\text{out}}}{P_{\text{in}}} = \frac{\kappa_R}{i(\omega_p - \omega) + \kappa_p + \frac{g^2}{i(\omega_m - \omega) + \kappa_m}}, \quad (1)$$

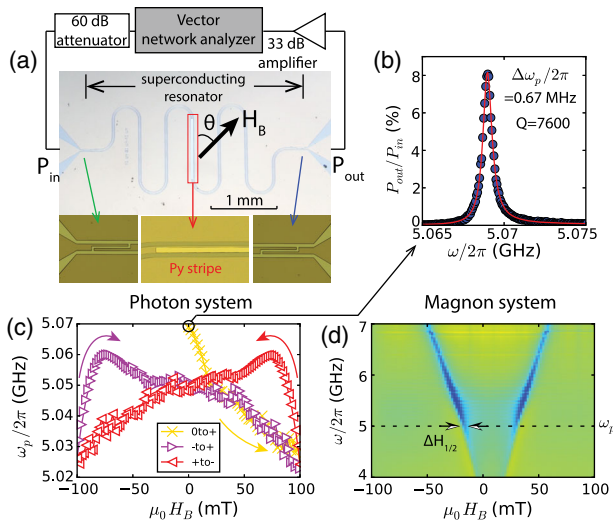


FIG. 1. (a) The microwave circuit of a NbN superconducting resonator with a Py stripe. The green (blue) and red boxes show the capacitive coupling to the external circuit and the Permalloy stripe, respectively. (b) Microwave power transmission of an unloaded superconducting resonator measured at $P_{\text{in}} = -55$ dBm after zero-field cooling. (c) Hysteresis evolution of ω_p for (b). (d) Ferromagnetic resonance spectra of a Py stripe measured at 1.4 K [38], with the linewidth at ω_p marked by arrows.

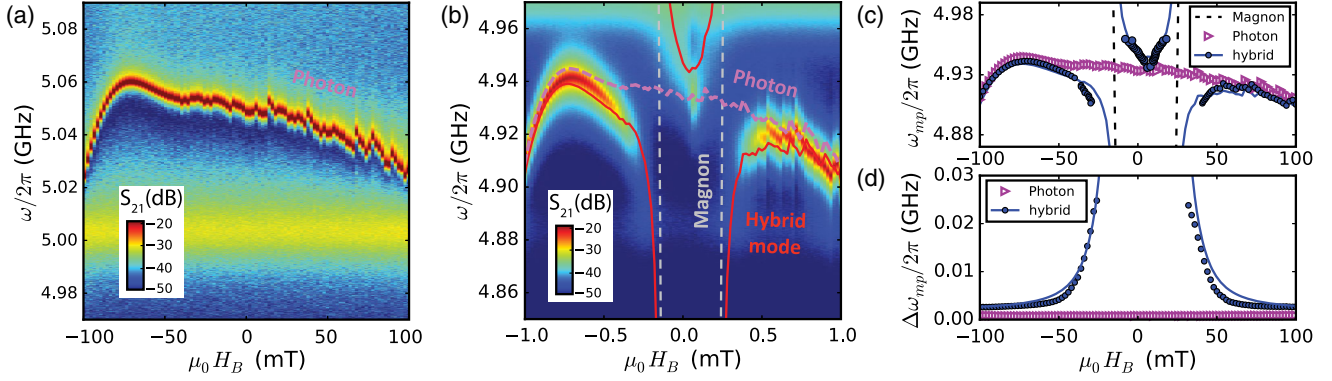


FIG. 2. Characterization of a 30-nm Py stripe ($L = 900 \mu\text{m}$) coupled to a NbN superconducting resonator, measured at $P_{\text{in}} = -55 \text{ dBm}$ and $\theta = 0^\circ$. (a)–(b) Microwave transmission spectra $S_{21} = 10 \log(P_{\text{out}}/P_{\text{in}})$ of (a) the unloaded resonator and (b) the resonator loaded with the Py stripe. (c) Extracted ω_{mp} and (d) $\Delta\omega_{mp}$ from (a)–(b). In (c) the photon modes have been shifted by -0.12 GHz to match the hybrid modes. Dashed lines denote the magnon modes. Solid blue and red curves denote the fits.

where κ_R is the capacitive coupling of the resonator to the external circuits and g is the magnon-photon coupling strength. With the additional Py load, $\kappa_p/2\pi$ is increased from 0.67 MHz to 2.0 MHz at $\mu_0 H_B = \pm 100 \text{ mT}$ [Fig. 2(d)]. Figure 2(c) overlays the fits to the eigenmode solution of Eq. (1) on top of the extracted ω_p from Fig. 2(b), with a single fit parameter $g/2\pi = 0.152 \text{ GHz}$ [38]. Note the large value of g despite the small ferromagnetic volume with merely 30 nm of Py. To understand the origin, the coupling strength is expressed as $g = g_0 \sqrt{N}$, where N is the total number of spins and $g_0 = \gamma \sqrt{\mu_0 \hbar \omega_p / V_c}$ is the coupling strength of the superconducting resonator to a single Bohr magneton. Here $\gamma/2\pi = (g_{\text{eff}}/2) \times 28 \text{ GHz/T}$ is the gyromagnetic ratio with $g_{\text{eff}} = 2.12$ the g factor for Py, \hbar is the Planck constant, and V_c is the mode volume of the resonator. Using the dimensions of the Py stripe and $\mu_0 M_s = 1 \text{ T}$ for the Py saturation magnetization, we calculate $N = 3.25 \times 10^{13}$ and $g_0 = 26.7 \text{ Hz}$ from the experiment. We highlight that our g_0 is 3 orders of magnitude larger compared with using a macroscopic cavity [14,15]. It comes from the small mode volume $V_c \sim 0.0051 \text{ mm}^3$ for the coplanar resonator and indicates the significance of having a localized and concentrated photon mode volume to reach a strong coupling strength. It is worthwhile to note a few different planar resonator designs such as split-ring [17,40,41] and lumped-element resonators [42,43]. The former allows an optimal filling of thin-film magnetic materials in the resonator, with $g/2\pi$ close to 1 GHz ; the latter has the highest g_0 by further reducing the mode volume. In addition, compared with the similar superconducting resonator structure coupled to a YIG slab [13] ($g/2\pi = 0.45 \text{ GHz}$, $g_0/2\pi = 2.5 \text{ Hz}$, and $N = 4 \times 10^{16}$), our g_0 is 1 order of magnitude larger because the Py device is in good proximity to the resonator and maintains optimal coupling efficiency. This yields a comparable g of Py stripe but with 3 orders of magnitude less number of

total spins than in the YIG slab. A large cooperativity of the hybrid system as $C = g^2 / \kappa_m \kappa_p = 68$ is obtained, which is a promising feature of coherent information exchange between photons and magnons in Py.

In addition to the frequency shift, we also observe a linewidth variation for the hybrid modes [19]. In Fig. 2(d), when $\mu_0 H_B$ is close to the anticrossing regime, $\Delta\omega_{mp}$ quickly increases from the photon damping rate $\kappa_p/2\pi = 2 \text{ MHz}$ and approaches the magnon damping rate κ_m . This is due to the mixing of relaxation channels when the magnon and photon modes are hybridized; see the Supplemental Material [38]. We plot the theoretical prediction in Fig. 2(d) with the same input values of g , κ_p , and κ_m in Fig. 2(c), and the linewidth of the hybrid modes can be reproduced. Between the two mode-crossing gaps (between -25 and $+32 \text{ mT}$) the hybrid modes are influenced by the saturation state of the Py stripe, which significantly deviate from the macrospin model and are not shown.

The coupling strength g is tunable by changing the dipolar coupling efficiency between magnons and photons as well as changing the total number of spins in Py. Figures 3(a)–3(d) show the microwave transmission spectra of the same device in Fig. 2 at different θ . As θ deviates from 0° , the mode anticrossing becomes smaller and disappears at 90° . This is due to the change of dipolar coupling energy, $E = \mu_0 M_\perp h_{rf} \cos \theta$, where the transverse components of the dynamic magnetization M_\perp and microwave field h_{rf} are no longer parallel and become orthogonal when $\theta = 90^\circ$. The extracted g can be modeled by a cosine function of θ (red curve) in Fig. 3(e). In addition, there are two additional observations in Figs. 3(a)–3(d): the mode anticrossing moves towards the lower biasing fields, and a spectral gap appears near $\mu_0 H_B = 0 \text{ mT}$ for $\theta = 90^\circ$. They are due to the shape anisotropy of the Py stripe [44], which pins the Py magnetization along $\theta = 0^\circ$ at low fields. To vary the total number of spins for magnons, we have

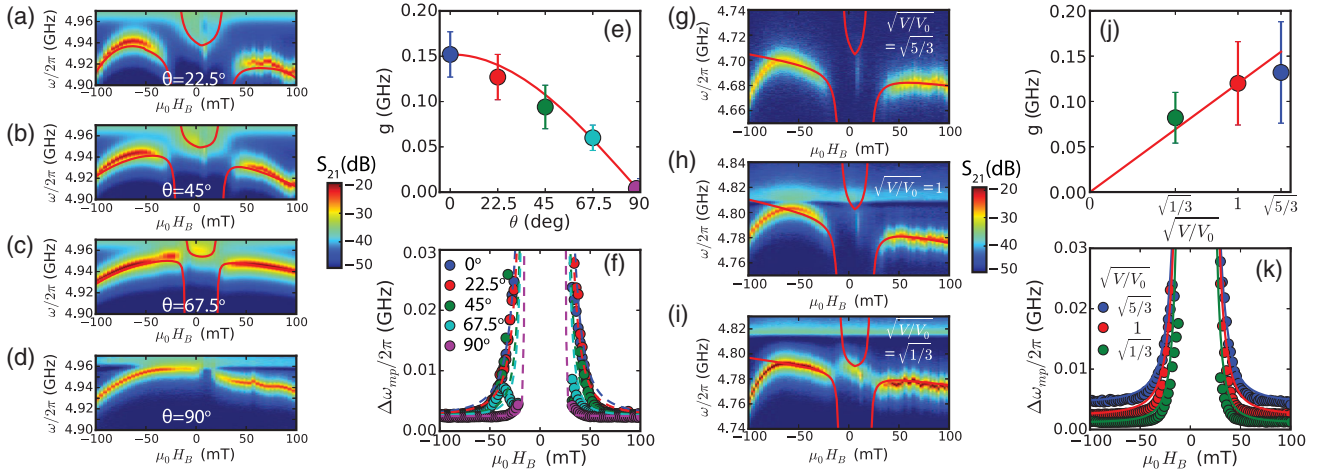


FIG. 3. Tunable magnon-photon coupling. (a)–(d) Microwave transmission spectra of the NbN superconducting resonator loaded with a Py(30 nm) stripe with $L = 900 \mu\text{m}$, from $\theta = 22.5^\circ$ to 90° . (e) Extracted coupling strength g as a function of θ with the fit. (f) $\Delta\omega_p$ as a function of $\mu_0 H_B$ with the dashed fits. (g)–(i) Transmission spectra for different Py stripes: (g) $t = 50 \text{ nm}$, $L = 900 \mu\text{m}$; (h) $t = 30 \text{ nm}$, $L = 900 \mu\text{m}$; (i) $t = 300 \text{ nm}$, $L = 900 \mu\text{m}$. (j) Extracted g as a function of $\sqrt{V/V_0}$, where V_0 denotes the volume of the Py(30 nm) stripe with $L = 900 \mu\text{m}$. (k) $\Delta\omega_p$ as a function of $\mu_0 H_B$, with the fitting curve also plotted.

fabricated a new series of Py stripes with different lengths (L) and thicknesses (t) and show their transmission spectra in Figs. 3(g)–3(i). As the coupling strength is reduced, the mode hybridization becomes weaker and for the smallest Py volume in Fig. 3(i), the spectra go into the Purcell regime [15] as g becomes significantly smaller than κ_m . In Fig. 3(j) a linear fit to $g = g_0\sqrt{N}$ is shown with a red line with an extracted $g_0/2\pi = 21.4 \text{ Hz}$, which is close to the value obtained in Fig. 2.

The evolution of $\Delta\omega_{mp}$ also changes accordingly for different magnon-photon coupling conditions. In Fig. 3(f) when the biasing field is far away from the anticrossing regime ($\mu_0 H_B = \pm 100 \text{ mT}$), $\Delta\omega_{mp}$ shows a consistent value of 2.5 MHz for the same Py device at different θ . As H_B approaches the anti-crossing conditions, $\Delta\omega_{mp}$ increases much slower for larger θ , because the coupling strength is decreasing. This trend can be reproduced in dashed curves by taking different values of g from Fig. 3(e) in the theoretical model [38]. In Fig. 3(k), due to the variation of the dielectric loss from Py, the values of κ_p are different, as 4.4, 2.3, and 1.1 MHz for Figs. 3(g)–3(i), respectively. By accounting for this κ_p variation, the linewidths can be also well fitted for different Py volumes.

Next, we show that the photon mode in the hybrid system can easily go into the nonlinear regime. This concept has been used for high-fidelity quantum operations [45–47]. In Fig. 4(a), we show the output line shapes of the superconducting resonator loaded with a Py(50 nm) stripe from $P_{\text{in}} = -15$ to 5 dBm, at $\mu_0 H_B = 100 \text{ mT}$ and $\theta = 0^\circ$. A nonlinear shift of the peak position towards the lower frequency is observed, with a critical power of $P_c = -5 \text{ dBm}$ for the line shape to reach a vertical slope [Fig. 4(b)]. This critical power is well below the typical threshold power for the magnon system alone to reach the

nonlinear regime [48]. The origin of the nonlinearity is the kinetic inductance variation of flux vortices [49] in the NbN resonator, which leads to frequency downshifts as also observed in Fig. 1(c) at increasing H_B . We note that such vortex-induced nonlinearity in the superconducting resonator can be extended to the variation of a single vortex flux [50], which shows potential for conducting operations in the quantum limit. The dynamics of magnetic flux vortices also leads to an increase of photon damping rate κ_p [51], reflected by the reduction of the maximal value of $P_{\text{out}}/P_{\text{in}}$ in Fig. 4(b).

Accompanied by the resonator nonlinearity, we also observe an enhanced magnon-photon coupling. In Fig. 4(c) we show the extracted peak positions of the hybrid mode for the 50-nm Py stripe. In the vicinity of the anticrossing

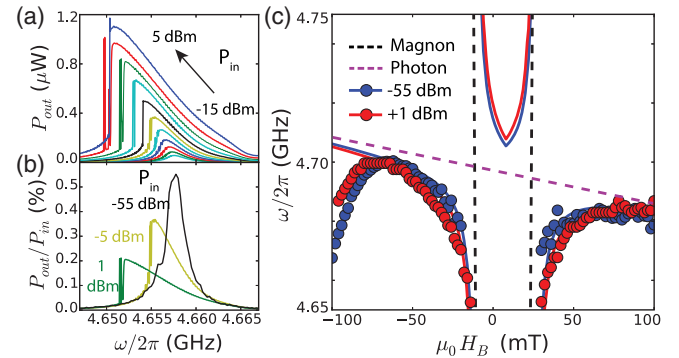


FIG. 4. Magnon-photon coupling in the nonlinear regime. (a) Nonlinear resonance line shapes from $P_{\text{in}} = -15$ dBm to $P_{\text{in}} = 5 \text{ dBm}$ with a step of 2 dB for Py(50 nm) stripe with $L = 900 \mu\text{m}$. (b) $P_{\text{out}}/P_{\text{in}}$ for $P_{\text{in}} = -55$, -5 , and 1 dBm . (c) Comparison of peak positions of the hybrid modes between $P_{\text{in}} = 1$ and -55 dBm .

regimes ($\mu_0 H_B$ close to the magnon branch), the peaks with $P_{\text{in}} = 1$ dBm show a stronger mode repelling compared with $P_{\text{in}} = -55$ dBm. Fitting the data to Eq. (1) yields a coupling strength of 0.158 GHz at 1 dBm input, which is 14% larger than the value of 0.139 GHz at -55 dBm, in Fig. 3(j). This coupling enhancement is likely caused by the Meissner field trapping from the dynamic flux vortices [52], which will influence the distribution of the magnetic field at the superconducting stripline and thus change the dipolar coupling strength with the Py magnon system. Therefore, the magnon-photon coupling may be also used as an effective means for detecting flux vortex dynamics in hybrid superconducting devices.

In conclusion, we have demonstrated a new hybrid platform consisting of a superconducting resonator and a ferromagnetic device integrated on a Si substrate. We obtained a large magnon-photon coupling strength of 0.152 GHz and a cooperativity of 68 for a 30-nm-thick Py stripe. We also show that the superconducting resonator can easily reach the nonlinear regime, in which the efficiency of the magnon-photon coupling is improved. Our results indicate that magnon-photon hybrid systems are promising as a high-speed and coherent transducer for realizing circuit quantum electrodynamics [24] in microscopic magnetic devices that are compatible with on-chip designs. In spintronics, magnon-photon hybrid systems allow for exploring novel physics [53–55] and provide a means to transmit spin excitations coherently at long distance with photon excitations [56,57], outperforming the currently reported micrometer propagation using pure spin currents [58] or spin waves [59]. Thus this demonstration of strong magnon-photon coupling in planar thin-film devices provides a crucial stepping stone for the development of more complex quantum information systems.

We acknowledge helpful discussions with Andy Kent and Xufeng Zhang. W. Z. acknowledges support from the U.S. National Science Foundation under Grant No. DMR-1808892 and the DOE-Visiting Faculty Program. Work at Argonne, including thin film synthesis, device fabrications, and low-temperature measurements, was supported by the U.S. Department of Energy (DOE), Office of Science, Materials Science and Engineering Division. Use of the Center for Nanoscale Materials, an Office of Science user facility, was supported by the U.S. Department of Energy, Office of Science, Office of Basic Energy Sciences, under Contract No. DE-AC02-06CH11357.

Note added in the proof.—Recently we became aware of closely related work by Hou *et al.* [60].

*novosad@anl.gov

†hoffmann@anl.gov

‡weizhang@oakland.edu

- [1] M. Wallquist, K. Hammerer, P. Rabl, M. Lukin, and P. Zoller, *Phys. Scr.* **T137**, 014001 (2009).
- [2] Z.-L. Xiang, S. Ashhab, J. Q. You, and F. Nori, *Rev. Mod. Phys.* **85**, 623 (2013).
- [3] G. Kurizki, P. Bertet, Y. Kubo, K. Mølmer, D. Petrosyan, P. Rabl, and J. Schmiedmayer, *Proc. Natl. Acad. Sci. U.S.A.* **112**, 3866 (2015).
- [4] A. Wallraff, D. I. Schuster, A. Blais, L. Frunzio, R.-S. Huang, J. Majer, S. M. Kumar, S. Abd Girvin, and R. J. Schoelkopf, *Nature (London)* **431**, 162 (2004).
- [5] J. Verdú, H. Zoubi, C. Koller, J. Majer, H. Ritsch, and J. Schmiedmayer, *Phys. Rev. Lett.* **103**, 043603 (2009).
- [6] D. I. Schuster, A. P. Sears, E. Ginossar, L. DiCarlo, L. Frunzio, J. J. L. Morton, H. Wu, G. A. D. Briggs, B. B. Buckley, D. D. Awschalom, and R. J. Schoelkopf, *Phys. Rev. Lett.* **105**, 140501 (2010).
- [7] Y. Kubo, F. R. Ong, P. Bertet, D. Vion, V. Jacques, D. Zheng, A. Dréau, J.-F. Roch, A. Auffeves, F. Jelezko, J. Wrachtrup, M. F. Barthe, P. Bergonzo, and D. Esteve, *Phys. Rev. Lett.* **105**, 140502 (2010).
- [8] X. Zhu, S. Saito, A. Kemp, K. Kakuyanagi, S.-i. Karimoto, H. Nakano, W. J. Munro, Y. Tokura, M. S. Everitt, K. Nemoto, M. Kasu, N. Mizuochi, and K. Semba, *Nature (London)* **478**, 221 (2011).
- [9] E. Verhagen, S. Deléglise, S. Weis, A. Schliesser, and T. J. Kippenberg, *Nature (London)* **482**, 63 (2012).
- [10] J. J. Viennot, M. C. Dartiailh, A. Cottet, and T. Kontos, *Science* **349**, 408 (2015).
- [11] A. Blais, R.-S. Huang, A. Wallraff, S. M. Girvin, and R. J. Schoelkopf, *Phys. Rev. A* **69**, 062320 (2004).
- [12] O. O. Soykal and M. E. Flatté, *Phys. Rev. Lett.* **104**, 077202 (2010).
- [13] H. Huebl, C. W. Zollitsch, J. Lotze, F. Hocke, M. Greifenstein, A. Marx, R. Gross, and S. T. B. Goennenwein, *Phys. Rev. Lett.* **111**, 127003 (2013).
- [14] Y. Tabuchi, S. Ishino, T. Ishikawa, R. Yamazaki, K. Usami, and Y. Nakamura, *Phys. Rev. Lett.* **113**, 083603 (2014).
- [15] X. Zhang, C.-L. Zou, L. Jiang, and H. X. Tang, *Phys. Rev. Lett.* **113**, 156401 (2014).
- [16] M. Goryachev, W. G. Farr, D. L. Creedon, Y. Fan, M. Kostylev, and M. E. Tobar, *Phys. Rev. Applied* **2**, 054002 (2014).
- [17] B. Bhoi, T. Cliff, I. S. Maksymov, M. Kostylev, R. Aiyar, N. Venkataramani, S. Prasad, and R. L. Stamps, *J. Appl. Phys.* **116**, 243906 (2014).
- [18] Y. Tabuchi, S. Ishino, A. Noguchi, T. Ishikawa, R. Yamazaki, K. Usami, and Y. Nakamura, *Science* **349**, 405 (2015).
- [19] L. Bai, M. Harder, Y. P. Chen, X. Fan, J. Q. Xiao, and C.-M. Hu, *Phys. Rev. Lett.* **114**, 227201 (2015).
- [20] D. Zhang, X. M. Wang, T. F. Li, X. Q. Luo, W. Wu, F. Nori, and J. Q. You, *NPJ Quantum Inf.* **1**, 15014 (2015).
- [21] Y. Cao, P. Yan, H. Huebl, S. T. B. Goennenwein, and G. E. W. Bauer, *Phys. Rev. B* **91**, 094423 (2015).
- [22] N. J. Lambert, J. A. Haigh, and A. J. Ferguson, *J. Appl. Phys.* **117**, 053910 (2015).
- [23] N. Kostylev, M. Goryachev, and M. E. Tobar, *Appl. Phys. Lett.* **108**, 062402 (2016).
- [24] D. Lachance-Quirion, Y. Tabuchi, S. Ishino, A. Noguchi, T. Ishikawa, R. Yamazaki, and Y. Nakamura, *Sci. Adv.* **3**, e1603150 (2017).

- [25] R. G. E. Morris, A. F. van Loo, S. Kosen, and A. D. Karenowska, *Sci. Rep.* **7**, 11511 (2017).
- [26] I. Boventer, M. Pfirrmann, J. Krause, Y. Schön, M. Kläui, and M. Weides, *Phys. Rev. B* **97**, 184420 (2018).
- [27] A. Imamoğlu, *Phys. Rev. Lett.* **102**, 083602 (2009).
- [28] J. H. Wesenberg, A. Ardavan, G. A. D. Briggs, J. J. L. Morton, R. J. Schoelkopf, D. I. Schuster, and K. Mølmer, *Phys. Rev. Lett.* **103**, 070502 (2009).
- [29] S. Probst, H. Rotzinger, S. Wünsch, P. Jung, M. Jerger, M. Siegel, A. V. Ustinov, and P. A. Bushev, *Phys. Rev. Lett.* **110**, 157001 (2013).
- [30] A. Hoffmann, *IEEE Trans. Magn.* **49**, 5172 (2013).
- [31] J. Sinova, S. O. Valenzuela, J. Wunderlich, C. H. Back, and T. Jungwirth, *Rev. Mod. Phys.* **87**, 1213 (2015).
- [32] O. Mosendz, J. E. Pearson, F. Y. Fradin, G. E. W. Bauer, S. D. Bader, and A. Hoffmann, *Phys. Rev. Lett.* **104**, 046601 (2010).
- [33] L. Liu, T. Moriyama, D. C. Ralph, and R. A. Buhrman, *Phys. Rev. Lett.* **106**, 036601 (2011).
- [34] H. Nakayama, M. Althammer, Y.-T. Chen, K. Uchida, Y. Kajiwara, D. Kikuchi, T. Ohtani, S. Geprägs, M. Opel, S. Takahashi, R. Gross, G. E. W. Bauer, S. T. B. Goennenwein, and E. Saitoh, *Phys. Rev. Lett.* **110**, 206601 (2013).
- [35] C. Liu, S. M. Wu, J. E. Pearson, J. S. Jiang, N. d'Ambrumenil, and A. Bhattacharya, *Phys. Rev. B* **98**, 060415 (2018).
- [36] M. Göppl, A. Fragner, M. Baur, R. Bianchetti, S. Filipp, J. M. Fink, P. J. Leek, G. Puebla, L. Steffen, and A. Wallraff, *J. Appl. Phys.* **104**, 113904 (2008).
- [37] T. Polakovic, S. Lendinez, J. E. Pearson, A. Hoffmann, V. Yefremenko, C. L. Chang, W. Armstrong, K. Hafidi, G. Karapetrov, and V. Novosad, *APL Mater.* **6**, 076107 (2018).
- [38] See Supplemental Material at <http://link.aps.org/supplemental/10.1103/PhysRevLett.123.107701> for details.
- [39] D. Bothner, T. Gaber, M. Kemmler, D. Koelle, R. Kleiner, S. Wünsch, and M. Siegel, *Phys. Rev. B* **86**, 014517 (2012).
- [40] B. Bhoi, B. Kim, J. Kim, Y.-J. Cho, and S.-K. Kim, *Sci. Rep.* **7**, 11930 (2017).
- [41] L. V. Abdurakhimov, S. Khan, N. A. Panjwani, J. D. Breeze, M. Mochizuki, S. Seki, Y. Tokura, J. J. L. Morton, and H. Kurebayashi, *Phys. Rev. B* **99**, 140401(R) (2019).
- [42] A. Bienfait, J. J. Pla, Y. Kubo, M. Stern, X. Zhou, C. C. Lo, C. D. Weis, T. Schenkel, M. L. W. Thewalt, D. Vion, D. Esteve, B. Julsgaard, K. Mølmer, J. J. L. Morton, and P. Bertet, *Nat. Nanotechnol.* **11**, 253 (2016).
- [43] C. Eichler, A. J. Sigillito, S. A. Lyon, and J. R. Petta, *Phys. Rev. Lett.* **118**, 037701 (2017).
- [44] Y. Li, Y. Lu, and W. E. Bailey, *J. Appl. Phys.* **113**, 17B506 (2013).
- [45] B. Yurke and E. Buks, *J. Lightwave Technol.* **24**, 5054 (2006).
- [46] F. Mallet, F. R. Ong, A. Palacios-Laloy, F. Nguyen, P. Bertet, D. Vion, and D. Esteve, *Nat. Phys.* **5**, 791 (2009).
- [47] F. R. Ong, M. Boissonneault, F. Mallet, A. Palacios-Laloy, A. Dewes, A. C. Doherty, A. Blais, P. Bertet, D. Vion, and D. Esteve, *Phys. Rev. Lett.* **106**, 167002 (2011).
- [48] Y.-P. Wang, G.-Q. Zhang, D. Zhang, T.-F. Li, C.-M. Hu, and J. Q. You, *Phys. Rev. Lett.* **120**, 057202 (2018).
- [49] M. A. Golosovsky, H. J. Snortland, and M. R. Beasley, *Phys. Rev. B* **51**, 6462 (1995).
- [50] I. Nsanzezeza and B. L. T. Plourde, *Phys. Rev. Lett.* **113**, 117002 (2014).
- [51] C. Song, T. W. Heitmann, M. P. DeFeo, K. Yu, R. McDermott, M. Neeley, J. M. Martinis, and B. L. T. Plourde, *Phys. Rev. B* **79**, 174512 (2009).
- [52] M. Taupin, I. Khaymovich, M. Meschke, A. Melnikov, and J. P. Pekola, *Nat. Commun.* **7**, 10977 (2016).
- [53] M. Harder, Y. Yang, B. M. Yao, C. H. Yu, J. W. Rao, Y. S. Gui, R. L. Stamps, and C.-M. Hu, *Phys. Rev. Lett.* **121**, 137203 (2018).
- [54] B. Bhoi, B. Kim, S.-H. Jang, J. Kim, J. Yang, Y.-J. Cho, and S.-K. Kim, *Phys. Rev. B* **99**, 134426 (2019).
- [55] I. Boventer, C. Dörflinger, T. Wolz, R. Macêdo, R. Lebrun, M. Kläui, and M. Weides, [arXiv:1904.00393](https://arxiv.org/abs/1904.00393).
- [56] X. Zhang, C.-L. Zou, N. Zhu, F. Marquardt, L. Jiang, and H. X. Tang, *Nat. Commun.* **6**, 8914 (2015).
- [57] L. Bai, M. Harder, P. Hyde, Z. Zhang, C.-M. Hu, Y. P. Chen, and J. Q. Xiao, *Phys. Rev. Lett.* **118**, 217201 (2017).
- [58] S. O. Valenzuela and M. Tinkham, *Nature (London)* **442**, 176 (2006).
- [59] Y. Kajiwara, K. Harii, S. Takahashi, J. Ohe, K. Uchida, M. Mizuguchi, H. Umezawa, H. Kawai, K. Ando, K. Takanashi, S. Maekawa, and E. Saitoh, *Nature (London)* **464**, 262 (2010).
- [60] J. T. Hou and L. Liu, [arXiv:1903.01887](https://arxiv.org/abs/1903.01887).